LBL-35113
UC-2000

ERNEST ORLANDO LAWRENCE
BERKELEY NATIONAL LABORATORY

Physical Barriers Formed From Gelling Liquids: 1. Numerical Design of Laboratory and Field Experiments

S. Finsterle, G.J. Moridis, K. Pruess, and P. Persoff
Earth Sciences Division

January 1994

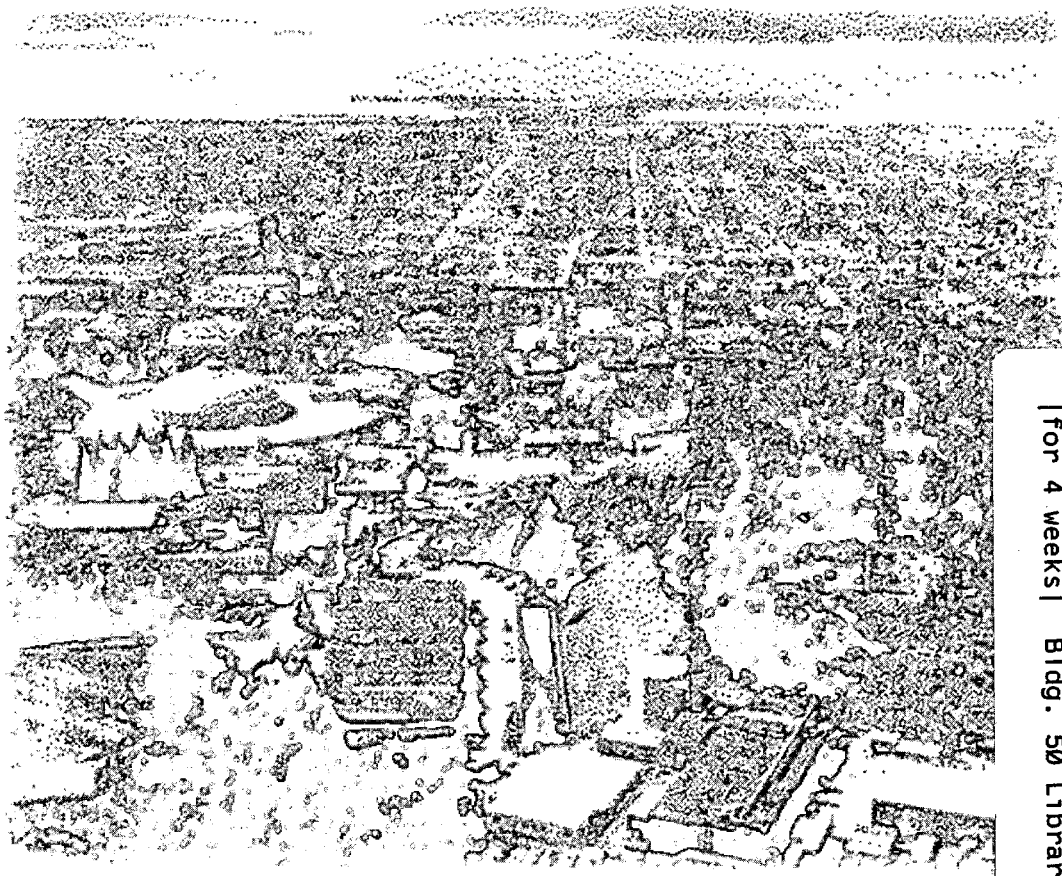

LOAN COPY
Circulates
for 4 weeks
Bldg. 50 Library.
Copy 2
LBL-35113

DISCLAIMER

This document was prepared as an account of work sponsored by the United States Government. While this document is believed to contain correct information, neither the United States Government nor any agency thereof, nor the Regents of the University of California, nor any of their employees, makes any warranty, express or implied, or assumes any legal responsibility for the accuracy, completeness, or usefulness of any information, apparatus, product, or process disclosed, or represents that its use would not infringe privately owned rights. Reference herein to any specific commercial product, process, or service by its trade name, trademark, manufacturer, or otherwise, does not necessarily constitute or imply its endorsement, recommendation, or favoring by the United States Government or any agency thereof, or the Regents of the University of California. The views and opinions of authors expressed herein do not necessarily state or reflect those of the United States Government or any agency thereof or the Regents of the University of California.

LBL-35113

UC-2000

Physical Barriers Formed From Gelling Liquids: 1. Numerical Design of Laboratory and Field Experiments

S. Finsterle, G. J. Moridis, K. Pruess, and P. Persoff

Earth Sciences Division
Lawrence Berkeley National Laboratory
University of California
Berkeley, CA 94720

January 1994

This work is supported by the U.S. Department of Energy, Office of Environmental Management, Office of Technology Development, under contract DE-AC03-76SF00098.

ABSTRACT

The emplacement of liquids under controlled viscosity conditions is investigated by means of numerical simulations. Design calculations are performed for a laboratory experiment on a decimeter scale, and a field experiment on a meter scale. The purpose of the laboratory experiment is to study the behavior of multiple grout plumes when injected in a porous medium. The calculations for the field trial aim at designing a grout injection test from a vertical well in order to create a grout plume of a significant extent in the subsurface.

In our modeling approach, the grout is treated as a miscible fluid the viscosity of which is a function of time and concentration of the gelling agent in the pore water. If a certain high viscosity is reached and the movement of the grout plume ceases, the gel is assumed to solidify instantaneously, leading to a new porous medium with reduced porosity and permeability.

The modeling of the laboratory experiment shows that the saturation within the immobilized grout plume may be significantly below one, leading to an incomplete ceiling of the pore space. However, when multiple injections are performed, relatively high conductive pathways are preferentially filled with grout, assuring a sufficient permeability reduction after the grout has cured.

Modeling the planned field test reveals that emplacement of a grout plume of a certain extent may require long injection times if the permeability of the soil is low. A low initial grout viscosity is essential to facilitate reasonable injection times. Comparing numerical simulation results and back-of-the-envelope calculations show that simple formulas are sufficiently accurate to obtain a first estimate of injection times and plume sizes. This is only true for low permeable soils where gravitational slumping and spreading of the plume due to capillary forces are not significant processes within the time frame of interest.

TABLE OF CONTENTS

Abstract iii
Table of contents iv
List of figures v
List of tables vi
1. Introduction 1
2. Barrier fluids 2
3. Modeling approach 4
3.1 Process description 4
3.2 Fluid properties 5
3.3 Soil characteristics 7
3.4 Solidification model 10
4. Design calculations for laboratory experiment 13
4.1 Objectives 13
4.2 Experimental setup 14
4.3 Test sequence 15
4.4 Results 17
4.4.1 Performance measure 17
4.4.2 Preflush 18
4.4.3 Primary grout injection 20
4.4.4 Redistribution 21
4.4.5 Solidification 23
4.4.6 Secondary grout injection 24
4.4.7 Final soil properties 26
5. Design calculations for field experiment 27
5.1 Objectives 27
5.2 Experimental setup 27
5.3 Back-of-the-envelope calculations 28
5.4 Soil characteristics 33
5.5 Results 34
6. Summary and concluding remarks 41

References 43

LIST OF FIGURES

Figure 1: Viscosity as a function of CS concentration and time 6
Figure 2: Capillary pressure and relative permeability functions for OK-1 sand 8
Figure 3: Schematic of sandbox 14
Figure 4: Laboratory experiment: Spatial discretization 14
Figure 5: Liquid flow field at the end of preflushing 18
Figure 6: Liquid saturation after preflushing 19
Figure 7: CS content after primary grout injection 20
Figure 8: Liquid saturation 4 hours after primary grout injection 22
Figure 9: CS content 4 hours after primary grout injection 22
Figure 10: Logarithm of permeability after solidification of primary grout plume 24
Figure 11: CS content immediately after secondary grout injection 25
Figure 12: CS content 5 hours after secondary grout injection 25
Figure 13: Logarithm of permeability after solidification of secondary grout plume 26
Figure 14: Schematic of borehole setup 27
Figure 15: Field experiment: Spatial discretization 28
Figure 16: CS grout injection time as a function of permeability and plume size 32
Figure 17: Liquid saturation and pressure after preflushing 36
Figure 18: Liquid saturation and CS content at the end of the grout injection period . . 37
Figure 19: Pressure distribution at the end of the grout injection period 38
Figure 20: Flow rates and total grout mass injected 38
Figure 21: Liquid saturation and grout content at the end of the gelling period 39
Figure 22: Permeability distribution after grout solidified 40

LIST OF TABLES

Table 1: Parameter set, standard deviations for estimation of prediction error 8
Table 2: Test sequence 14
Table 3: Preflush: Performance measures and prediction errors 18
Table 4: Primary grout injection: Performance measures and prediction errors 20
Table 5: Redistribution: Performance measures and prediction errors 20
Table 6: Parameter ranges for scoping calculations 29
Table 7: Injection times required for each test period 30
Table 8: Reasonable parameter set leading to reduced injection times 30
Table 9: Correction factors to calculate injection times 31
Table 10: Parameter set for field experiment 33
Table 11: Model results field experiment 34

1. INTRODUCTION

The development of effective in situ contaminant containment technologies is necessitated by (a) the need to control and/or suppress the release of contaminants from buried sources, (b) the need to prevent the spread of existing plumes, and (c) the inability to effectively remove contaminants from the subsurface. Contaminants from buried wastes or from contaminated soils in the vadose zone can be mobilized and migrate toward previously uncontaminated regions of the aquifer. Underground storage facilities for hazardous wastes may be subject to leakage and/or leaching. Contaminants cling tenaciously to subsurface materials (especially clays), and traditional physical extraction methods are slow and ineffective. Excavation of contaminated soils and disposal in protected facilities is expensive and often impractical. Containment on-site and control of the groundwater flow pattern can limit the off-site threat, and may supply a long-term solution. In areas where complete control is necessary, impermeable barriers are preferable to sorption barriers. Moreover, a variety of barrier fluid technologies must be developed for different soil and waste-type conditions.

Despite the obvious need, containment technologies have been largely limited to expensive "brute-force" approaches involving trenching, and cut-off and slurry walls. The effectiveness of these methods is limited. This investigation is intended to address a knowledge gap in this area, and provide powerful and more economical containment methods with broad applicability in a large variety of sites. Moreover, these can be applied without excavation in areas afflicted by a wide range of contaminant problems (ranging from immiscible organic contaminants to solutes to heavy metals to mixed wastes) on both a temporary and a permanent basis.

There are three ways to apply the containment technology. The first, conditions permitting, results in a permanent immobilization of the contaminants by sealing and entombing them in a "monolith" of inert and impermeable material. This represents a radical deviation from the current approaches which either allow the contaminants in a free state and seek to reduce their rate of migration by reducing the permeability of the porous medium, or attempt to neutralize them through a chemical reaction. In the second option, an inert impermeable "cage" is created to surround and isolate the contaminated area, which can be treated at a later time. Alternatively, such a "cage" could enhance or even make possible remediation techniques (such as soil flushing) which currently face regulatory approval problems due to concerns about contaminants escaping into previously unaffected areas of

the subsurface. Finally, the third option allows sealing of permeable aquifer zones, thus helping to concentrate the effects of traditional cleanup techniques (such as pump and treat) in inaccessible and difficult-to-treat less permeable zones.

2. BARRIER FLUIDS

We examine liquids which, when injected into the subsurface, produce nearly-inert impermeable barriers through a very large increase in viscosity. Appropriate emplacement of these substances provides an effective containment of the contaminated zone by entrapping and immobilizing both the contaminant source and the plume.

Two general types of fluids are investigated. The increase in viscosity in the first type of fluids is provided by a gelation process. The barrier fluids are injected into the subsurface at ambient temperatures, and the sealing gel forms after a controlled gel time. In the second type the increase in viscosity is caused by a vulcanization-like process which results in the cross-linkage of the injected substances and the formation of a matrix of infinite viscosity. The cross-linking process is achieved by temperature control of the injected substances.

The first type is Colloidal Silica (CS), which is a silicon-based chemical grout. It poses no health hazard, is unaffected by filtration, is chemically and biologically inert, has excellent durability characteristics, and is injected isothermally. Its containment performance is controlled by the gel time, which depends on pH, temperature, the chemistry of the injected suspension, and chemistry and mineralogy of the aquifer porous medium. This material has been previously investigated in the oil industry for the sealing of "thief zones " in petroleum reservoirs.

The second type of barrier fluids belongs to the PolySiloXane (PSX) family, which are crosslinked polymers similar to RTV rubbers. PSXs are mixtures of two fluids, are chemically and biologically inert silicon-based polymers, are unaffected by the aquifer or waste chemistry, and their containment performance depends on temperature and the ratio of the two constituents. PSX have been used as materials for medical implants, as well as carriers for a variety of medicines injected into the human body, and a wealth of information is available on their non-toxicity. There is very recent information (September 1993) which indicates PSX use to provide water repellence, increase in mechanical strength, and inhibit

the penetration of destructive agents in the restoration of stone statues in archaeological restorations.

The theory of gelling of CS is discussed by *Iler* [1979]. Essentially, the negatively charged colloidal particles are surrounded by an electrical double layer of cations. When the ionic strength of the colloidal is increased, the double layer is compressed, allowing the particles to approach each other more closely and form Si-O-Si bonds, networks of particles form a gel. Control of the gel time is necessary for grout emplacement. The gel time of CS grouts increases with increasing pH and with decreasing ionic strength. Salt solutions are added to the colloid to increase the ionic strength and control gel time. When injected into soils with high ion exchange capacity, the gelling of CS grouts is significantly accelerated. This effect results from salinity that is present in pore water and from multi-valent ions that are desorbed from clays and ion-exchanged for mono-valent ions in the grout. These ions have to be removed prior to grout injection by preflushing the soil with a NaCl solution. The gel time of PSX grouts is controlled by the amount of the catalyst used, as well as temperature, but is unaffected by the soil chemistry which allows for direct grout injection without preflushing the soil.

When grout is injected into unsaturated soil it slumps, leaving the soil only partially saturated and achieving less permeability reduction upon gelling. Multiple injections of CS grout in sand columns demonstrated that by accumulating the residual gelled grout saturations from several injections, low permeability can be achieved.

The laboratory work performed to identify the barrier fluid and its application mode is reported in *Moridis et al.* [1994].

3. MODELING APPROACH

3.1 Process Description

Model development essentially consists of approximating the relevant factors that control the behavior of the system to be studied. In this Section we describe the modeling approach we have chosen to simulate the grout injection experiment. We outline the processes our model takes into account, and critically discuss the assumptions and simplifications that are made.

Injection of CS grout into an unsaturated porous medium leads to a system which consists of grains, a non-condensable gas, and an aqueous phase of variable CS concentration. Two major assumptions are made. First, the chemical process of gelation is not explicitly modeled. Instead, we calculate the viscosity of the aqueous phase as a function of CS concentration and time, based on laboratory data (see Section 3.4). Secondly, the grout is treated as an aqueous solution, i.e. the grout does not form a separate phase. This is a correct description at early times when grout and water are completely miscible. After a certain time, however, when the gelling process is initiated, the grout starts to form a separate phase, which turns into a non-Newtonian, visco-elastic fluid and eventually solidifies. The appearing of new phases is accompanied by a change of their physical and chemical properties as time proceeds. Contact angles and interfacial tensions vary with the chemical properties of the gel-water mixture, filtration and adsorption of gel clusters may occur, and by the time the grout is completely gelled, a new porous medium has been created with lower porosity and reduced permeability.

(1) The system is modeled as a porous medium with three phases (gas, liquid, and solid), and four components (air, water, CS, and sand). The viscosity of the liquid phase is a function of CS concentration and time (see Section 3.3).

(2) After completion of the gelling process, we assume that the grout (which is still a fluid of very high viscosity) solidifies instantaneously. By doing so, the porosity is reduced, and a new porous medium is formed which has a lower permeability and different characteristic curves in the region affected by the grout. The model describing the transition of the grout from a high viscous fluid to a solidified part of the matrix is discussed in Section 3.4.

The model calculations are carried out using the TOUGH2 code [*Pruess*, 1991a] with equation-of-state module EOS7 for two-phase flow of traced water and air [*Pruess*, 1991b].

Non-isothermal flow in multi dimensions is calculated in TOUGH2 by means of integrated finite differences. Dispersion and diffusion of grout in the liquid phase is not explicitly considered. However, the simulation exhibits numerical dispersion effects due to finite space and time discretization. Two types of numerical dispersion have to be considered. First, saturation profiles display enhanced smearing due to numerical dispersion which acts as an additional capillary force. Secondly, the grout concentration in the liquid phase also disperses numerically. Note that there is physical evidence for both dispersion effects (see e.g. *Pruess* [1991c, 1993]). A relatively fine mesh is built in order to reduce numerical dispersion effects.

3.2 Fluid Properties

The pore space is occupied by two fluids: the gaseous phase, air and water vapor, and the liquid phase which consists of water, CS, and dissolved air. The gaseous phase is treated as ideal, and additivity the vapor partial pressure is assumed. Dissolution of air in the liquid phase is represented by Henry's law. Thermophysical properties of liquid water and vapor are taken from steam table equations, as given by the *International Formulation Committee* [1967]. The increase of viscosity as a function of CS concentration and time is based on laboratory data and a simple mixing rule. The viscosity of colloidal silica was measured as a function of time using a viscometer. An exponential function was fitted to the data collected during the first hour after the gelling process has been initiated. The reason for selecting early time data is that the flow behavior of the grout plume is determined by the initial, relatively low viscosity of the grout, when the location and the shape of the grout plume is affected by gravity and capillary forces. The gel-time curve gives the viscosity of pure CS grout as a function of time:

Gel-Time Curve: $$\mu_{CS} = a_1 + a_2 \cdot \exp(a_3 \cdot t) \qquad (1)$$

The coefficients a_1 through a_3 are determined by fitting the model to data measured in the laboratory. After injection, the grout suspension will be diluted due to mixing with pore water. The following mixing rule is applied to calculate the viscosity increase as a function of CS concentration and time:

Mixing Rule: $$\mu_l = X_l^{CS} \cdot \mu_{CS} + (1 - X_l^{CS}) \cdot \mu_w \qquad (2)$$

where

μ_{CS} = viscosity of Colloidal Silica grout

μ_w = viscosity of water

μ_l = viscosity of liquid phase (gel-water mixture)

X_l^{CS} = CS mass fraction in liquid phase

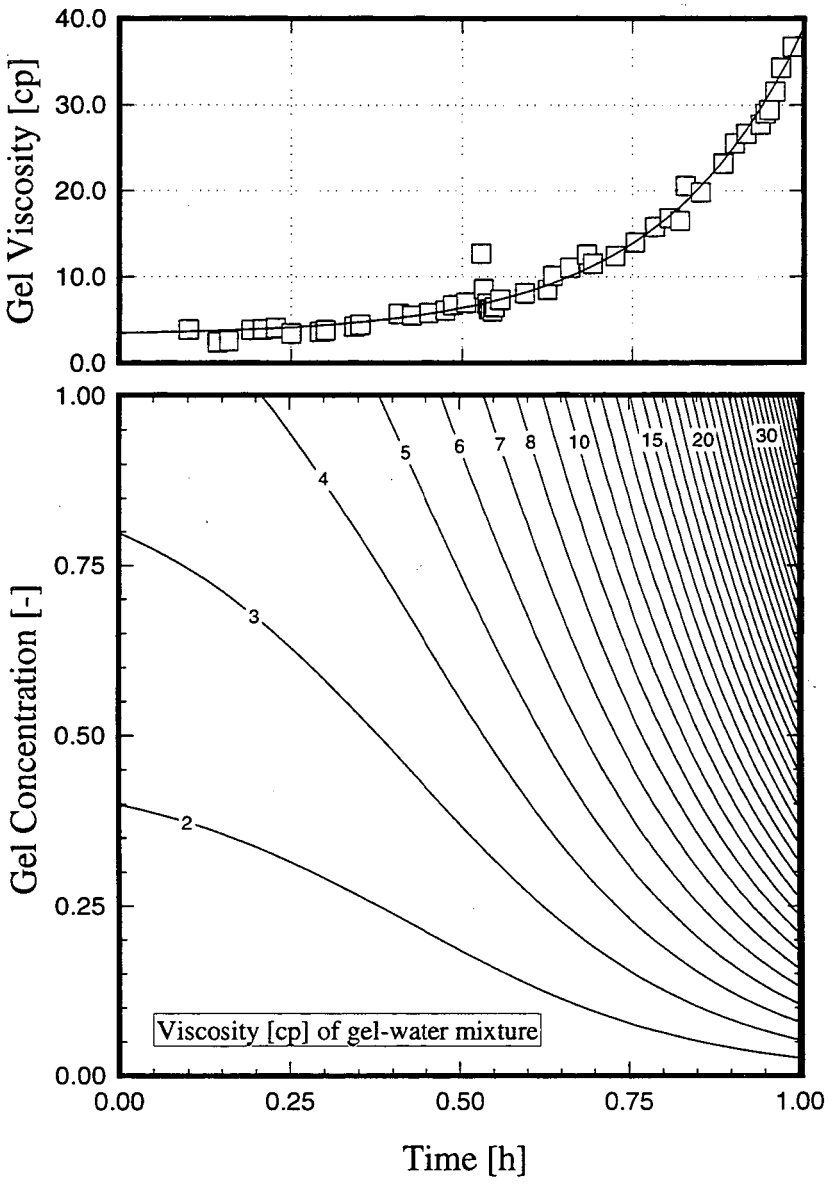

Figure 1: Viscosity as a function of CS concentration and time

The upper part of Figure 1 shows the laboratory data (symbols) and the gel-time curve (Equation 1) which corresponds to the viscosity increase as a function of time for CS

concentration $X_l^{CS} = 1$. The mixing rule (Equation 2) is visualized in the lower part of the Figure where viscosity of the liquid phase is contoured as a function of CS concentration and time.

Recall that the gel-time curve and the mixing rule are only meaningful as long as the grout is treated as a fluid. If solidification takes place by redefining the characteristics of the grouted soil, the CS concentration in the liquid phase has to be reset to zero, and a new gel-time curve has to be used.

3.3 Soil Characteristics

A laboratory experiment has been designed to study the emplacement and the performance of multiple grout plumes injected into partially saturated sand (see Section 4). Grout will be injected into Oklahoma #1 sand (OK-1). Its grain density was measured to be 2670 kg/m^3. The sand was slowly poured into the experiment tank. From the mass and bulk volume, and the sand grain density, the porosity was estimated 36 %. The saturated permeability of a representative sandpack was measured to be $8.0 \cdot 10^{-12}$ m^2. Data from a desorption experiment were used to determine the parameters of Brooks-Corey's capillary pressure function [*Brooks and Corey*, 1964]. Relative permeability functions are obtained based on Burdine's pore connectivity model [*Burdine*, 1953]. The characteristic curves are given by Equations (3) - (6) and shown in Figure 2.

$$p_c = p_e \cdot S_e^{-1/\lambda} \tag{3}$$

$$k_{rl} = S_e^{\frac{2+3\lambda}{\lambda}} \tag{4}$$

$$k_{rg} = (1 - S_e)^2 \cdot \left(1 - S_e^{\frac{2+\lambda}{\lambda}}\right) \tag{5}$$

with

$$S_e = \frac{S_l - S_{lr}}{1 - S_{lr}} \tag{6}$$

In this form, Brooks-Corey's curves contain three adjustable parameters: p_e (air entry pressure), λ (pore size distribution index), and S_{lr} (residual liquid saturation). S_e is effective liquid saturation.

The parameter values are summarized in Table 1. In the third column, a prior standard deviation is assigned to each of the input parameters for calculating prediction errors (see Section 4.4.1). The sensitivity measure (column 4) is the calculated as the sum of all sensitivity coefficients, multiplied with the prior standard deviation, and normalized to the sensitivity of the absolute permeability. A high value indicates that the quality of the model prediction can be greatly improved if the uncertainty of the corresponding input parameter is reduced. For example, the initial moisture content does not greatly affect the performance of the grout plume. This is basically due to the fact that the soil is preflushed with water, leading to an almost fully liquid saturated environment around the injection wells. On the other hand, absolute permeability is an important parameter which defines the size, location, and shape of the final grout plume. Note that the sensitivity values given in Table 1 cannot be generalized since they depend on the test layout, the definition of appropriate performance measures, and the assumptions regarding the prior errors of the input parameters (for more details see Section 4.4.1).

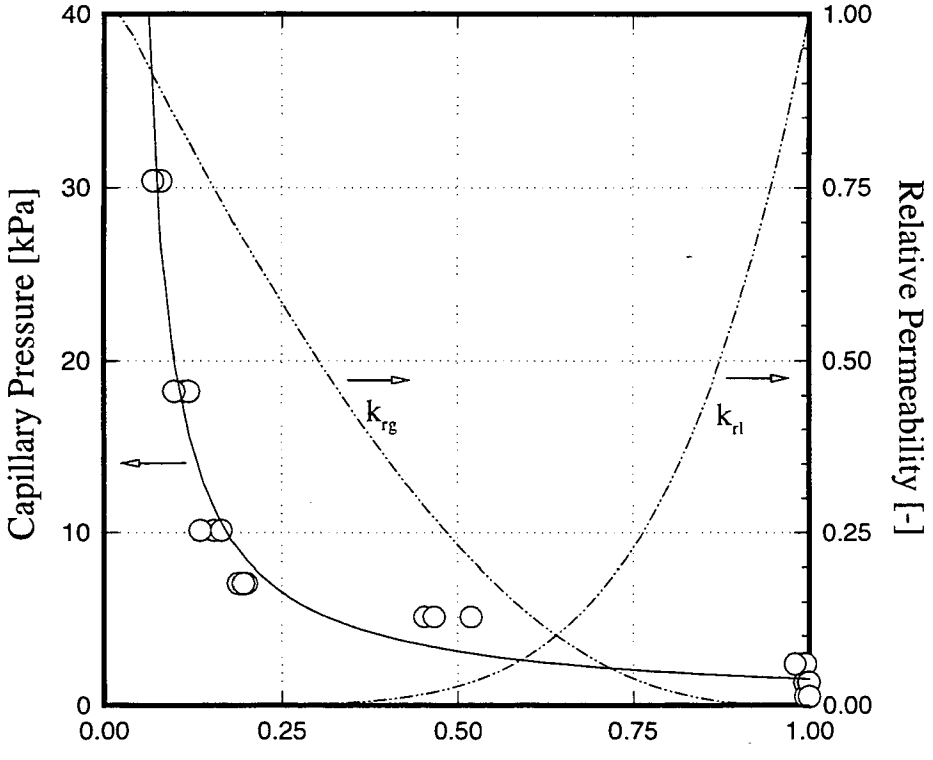

Figure 2: Capillary pressure and relative permeability functions for OK-1 sand

Parameter	Value	Std. dev.	Sensitivity
log (abs. permeability [m^2])	-11.10	0.20	1.00
porosity ϕ [-]	0.36	0.03	0.05
initial gas saturation S_{g0} [-]	0.95	0.05	0.02
injection pressure p_i [cm]	20.00	5.00	0.23
Characteristic curves: Brooks-Corey			
air entry pressure p_d [kPa]	1.70	0.25	0.18
pore size distribution index λ [-]	1.00	0.25	0.08
residual liquid saturation S_{lr} [-]	0.03	0.05	0.33
Grout characteristics			
Gel-time curve: a_1 [cp]	3.22	1.00	0.16
Gel-time curve: a_2 [cp]	0.28	0.10	0.13
Gel-time curve: a_3 [1/h]	4.84	1.00	0.12

Table 1: Parameter set, standard deviations for estimation of prediction error

3.4 Solidification Model

The grout is modeled as a fluid, the viscosity of which increases with time as gelation proceeds. However, the fact that a new phase evolves, initially as a separate liquid phase, but eventually as a solid forming a new porous medium, is not explicitly accounted for because the characteristics of this new phase, especially its wetting properties, are continuously changing with time and are difficult to determine. However, the properties of the new porous medium after complete solidification of the grout can be more easily described. The Solidification Model presented inhere gives the new parameter set for the grouted sand. The parameters to be recalculated are porosity, permeability, relative permeability and capillary pressure functions, and initial liquid saturation. They are basically a function of the final grout content in the sand. Note that an initially homogeneous sand becomes heterogeneous with lower porosities and permeabilities in regions with a high grout content. On the other hand, an initially heterogeneous sand may become more homogeneous on a scale smaller than the plume size, because highly permeable features are preferentially clogged with grout compared to regions which are already relatively impermeable.

The Solidification Model is based on the assumption that all the liquid in the pore space eventually solidifies if a certain CS concentration X_{sol} is exceeded. We introduce a parameter A as follows:

$$A = 1 \qquad \text{for} \quad X_l^{CS} \geq X_{sol} \tag{7}$$

$$A = \frac{X_l^{CS}}{X_{sol}} \qquad \text{for} \quad X_l^{CS} < X_{sol} \tag{8}$$

If we assume that all the liquid with a CS concentration greater than 0.2 eventually solidifies, X_{sol} is set to 0.2. The fluid with lower CS concentrations solidifies only partly, and the properties of the remaining liquid are reset to those of pure water. The liquid saturation at the time solidification occurs is denoted $S_{l,sol}$. The liquid saturation in the region with high gel contents is almost constant due to the high viscosity of the pore fluid. The Solidification Model is a set of equations, defining the hydrogeologic parameters of the grouted sand. The parameters subjected to the Solidification Models are porosity, absolute permeability, capillary pressure function, liquid saturation, and CS concentration.

The porosity of the grouted sand is reduced by the amount of gel that solidified:

$$\phi_{new} = \phi_{old}\,(1 - A \cdot S_{l,sol}) \tag{9}$$

The porosity reduction leads to an appropriate decrease of absolute permeability which is the mechanism that forms the impermeable layer designed to be the subsurface barrier. The partial clogging of the pore space by grout is conceptually similar to the permeability reduction due to phase interferences in a multiphase flow system. Therefore, we take the relative permeability function of the non-wetting phase to calculate the absolute permeability of the grouted sand:

$$k_{new} = k_{old} \cdot \left[1 - A \cdot (1 - k_{rg}(S_{l,sol}))\right] \tag{10}$$

The permeability reduction might in fact be stronger, because not only are the small pores sealed by the wetting grout, but deposition of gel at the pore walls also reduces the diameter of the remaining larger pores. Laboratory experiments with multiple injections of grout and subsequent permeability measurements indicate that permeability reduces by the fourth power of the effective, non-wetting phase saturation [*Moridis et al.*, 1993].

The capillary pressures of the grouted sand is expected to be more negative for a given water content. We apply Leverett's model to calculate the capillary strength of the medium with reduced permeability. At the same time, saturations have to be scaled to the new porosity and liquid saturation of the sand:

$$p_{c,new}(S_l) = p_{c,old}(S_{l,ori}) \cdot \sqrt{\frac{k_{old}}{k_{new}}} \tag{11}$$

where

$$S_{l,ori} = A \cdot S_{l,sol} + S_l \cdot \frac{\phi_{new}}{\phi_{old}} = A \cdot S_{l,sol} + S_l \cdot (1 - A \cdot S_{l,sol}) \tag{12}$$

Given a certain liquid saturation S_l of the grouted sand, Equation (12) recalculates the original liquid saturation $S_{l,ori}$ to obtain the corresponding capillary pressure, which is enhanced by applying Leverett's scaling model, Equation (11).

The liquid saturation after solidification is the volume of the ungelled pore fluid divided by the new pore volume from Eq. (9):

$$S_{l0,new} = \frac{S_{l,sol} \cdot (1 - A)}{1 - A \cdot S_{l,sol}} \tag{13}$$

Finally, the gel concentration in the unsolidified fluid is recalculated:

$$X_l^{CS}{}_{new} = (1 - A) \cdot X_l^{CS}{}_{old} \tag{14}$$

Note that if new gel time curves are applied (e.g. for modeling a secondary grout injection), the residual gel content from a previous injection behaves like newly injected grout. This usually small amount of grout, however, resides mainly at the disperse interface between the grouted region and the zone which is not affected by gelation.

The Solidification Model has to be applied to each grid block of the discretized flow region to provide initial conditions and sand properties for subsequent simulations.

Needless to say that the Solidification Model proposed herein is highly speculative. A laboratory experiment has to be designed to actually measure the characteristics of the porous medium after complete gelling of the injected grout. Reducing the permeability of the sand is the means by which the release and spread of contaminants from buried sources is suppressed. Assessing the Solidification Model is therefore an essential requirement for a containment technology which is based on the emplacement of liquids under controlled viscosity conditions.

4. Design Calculations for Laboratory Experiment

4.1 Objectives

Model calculations are performed to design a laboratory experiment in a tank filled with sand. The objective of the experiment is to investigate the placement and the performance of one or multiple grout plumes injected into partially saturated sand. The following requirements and restrictions apply:

- Two primary and one secondary grout plumes are to be created from horizontal wells
- The size of the individual plumes shall be large enough to allow for subsequent coring and testing
- The size of the individual plumes shall be small enough in order to avoid boundary effects
- The distance between the primary wells as well as the plume size shall be designed such that the two plumes merge
- Injection rates during preflushing and grout injection shall be small in order to avoid large overpressures and unstable displacement
- Grout injection time shall be short compared to gelling time
- Gel time shall be short enough in order to avoid the plume reaching the bottom of the sandbox

The experiment is basically limited by the dimensions of the tank (see Section 4.2) which in turn restrains the time scale for injection, redistribution and curing of the grout. Some effects seen in the experiment may not be important on a lager scale (e.g. wall effects) whereas some effects which are significant on a larger scale cannot be appropriately reproduced in the tank (e.g. slumping of the grout plume under gravity). Consequently, scale effects have to be considered when interpreting modeling results and observations from the laboratory experiment.

4.2 Experimental Layout

The dimensions of the tank are 50.0 × 18.0 × 25.0 cm. Three horizontal holes are drilled as shown in Figure 3. The two lower holes are used for a primary grout injection, the third borehole centered above is used for a secondary injection. The corresponding finite difference grid is shown in Figure 4. Note that only half of the sandbox needs to be modeled because of a vertical symmetry plane.

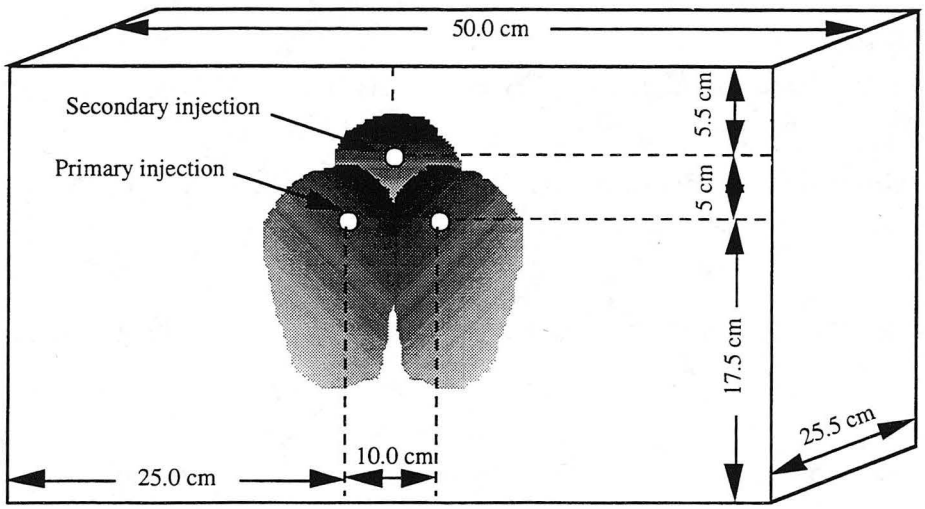

Figure 3: Schematic of sandbox

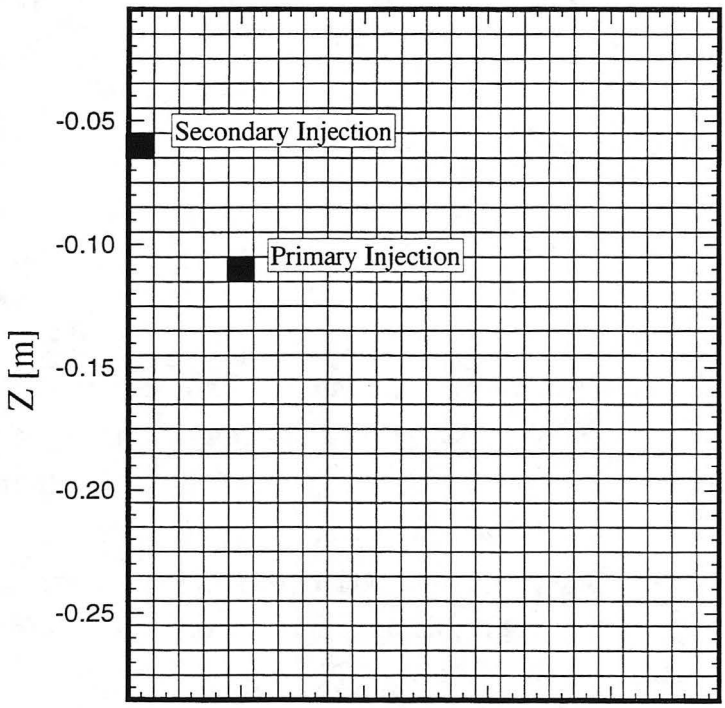

Figure 4: Laboratory experiment: Spatial discretization

4.3 Test Sequence

The test sequence summarized in Table 2 has been found to be appropriate in order to meet the objectives of the experiment:

Test Phase	Duration [min]	Time [hh:mm]	Comment
Preflush	45	00:45	Inject at 2.0 kPa overpressure
1. grout injection	8	00:53	Inject at 2.0 kPa overpressure
Redistribution	247	05:00	Stop injection
Solidification	0	05:00	Apply Solidification Model
2. grout injection	10	05:10	Inject at 1.5 kPa overpressure
Redistribution	290	10:00	Stop injection
Solidification	0	10:00	Apply Solidification Model

Table 2: Test sequence

Preflush

The chemical behavior of CS grouts is influenced by the presence of multi-valent ions in the soil and soil-water which tend to greatly accelerate the gelation process. A controllable gel time is an essential requirement for successful emplacement of the grout in the subsurface. The ions preferentially adsorbed at the clay particles are removed by flushing the soil with water and, more effectively, by a 4% NaCl solution. It has been shown [*Moridis et al.*, 1994] that the pre-treatment of the soil results in controllable gel times. Notice that no preflushing is required for Polysiloxene grouts. In the laboratory experiment, water and NaCl solution is injected at by applying a constant overpressure of 2.0 kPa for 45 minutes.

Primary grout injection

Preflushing is stopped and immediately followed by the injection of CS grout. After 8 minutes, about 0.75 kg of grout has been injected per borehole. The viscosity of the grout starts increasing according to the gel-time curve and mixing rule discussed in Section 3.2.

Redistribution

Grout injection stops, and the grout plume is allowed to redistribute, driven by gravity and capillary forces. The viscosity of the grout-water mixture increases with time.

Solidification

Five hours after the beginning of the experiment, the saturation distribution has almost reached steady-state conditions due to the high viscosity of the grout. At this point, we apply the Solidification Model and redefine the properties of the grouted sand.

Secondary grout injection

Preliminary studies have shown that multiple injections of grout are required to achieve nearly impermeable barriers [*Moridis et al.*, 1994]. The injection of a secondary grout plume aims at further reducing the permeability of the grouted sand.

Redistribution

The secondary grout plume is allowed to slump and spread for 190 minutes.

Solidification

The Solidification Model is applied to calculate the final properties of the grouted sand.

Each test period will be discussed in detail in the following Sections.

4.4 Results

4.4.1 Performance measure

In order to easily report the results of the numerical simulation, we define a set of performance measures which are considered representative for the behavior of the grout plume:

(1) Total grout mass in place
(2) Average liquid saturation S_l in the region around the primary injection well.
(3) First moment of grout content = center of grout mass (X and Z-coordinate)
(4) Second moment of grout content = spreading of grout plume in X and Z direction

Note that the liquid phase contains two-components: water and grout. The grout plume is defined by the region where $X_l^{CS} > 0$. The grout content is defined as the product of grout concentration and liquid saturation. We will also show contour plots of liquid saturation, grout content, gas pressure, as well as maps of the permeability field.

A prediction error will be calculated for each of the performance measures, based on the standard deviations assigned to each input parameter (see Table 1). The latter provide the diagonal elements of covariance matrix **C**. Furthermore, a sensitivity matrix **J** is calculated with elements $J_{ij} = \partial q_i/\partial p_j$, where q_i is the i-th performance measure (e.g. plume location), and p_j is the j-th parameter (e.g. parameter a_1 of gel-time curve). The prediction error (square root of diagonal elements of matrix $\mathbf{C}_{sim}$) is then estimated using linear error analysis:

$$\mathbf{C}_{sim} = \mathbf{J}\,\mathbf{C}\,\mathbf{J}^T \tag{15}$$

Equation (15) is based on the assumption that the probability density function of the input parameters is normal (and can therefore be summarized in covariance matrix **C**), and that the model output can accurately be approximated by a linear function of the parameters within the confidence region of interest. We will see that, based on these assumptions, a certain (usually low) probability is assigned to plume locations which are physically not possible. This illustrates the limitations of the linear error analysis. We believe, however, that linear error analysis is accurate enough to estimate prediction uncertainties of the design calculations.

4.4.2 Preflush

The sand is initially almost dry with a uniform liquid saturation of 5 % which is equivalent to a capillary suction of -58.7 kPa. The bottom of the tank is in contact with a larger volume of sand which maintains the capillary suction at the lower boundary. The top of the tank is open, and humid air is allowed to enter the sand. No flow boundary conditions are applied at the left and right of the model domain. Recall that the left boundary is a symmetry plane. Initial gas pressure is 100 kPa; initial liquid pressure is 41.3 kPa.

Water is injected at a constant pressure of 102 kPa for 45 minutes. Figure 5 illustrates the radial flow field around the injection well, overlaid by a relatively small downward flux of water due to gravity.

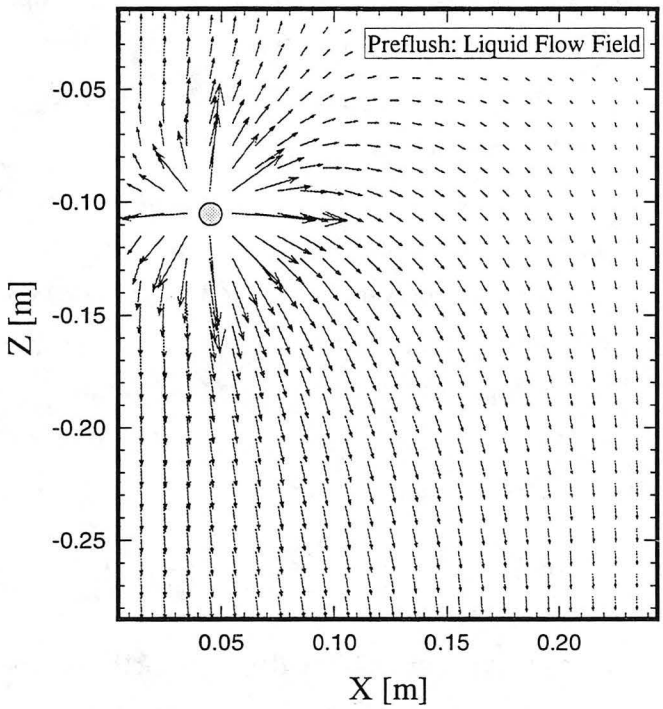

Figure 5: Liquid flow field at the end of preflushing

Contours of liquid saturation at the end of the preflushing period are shown in Figure 6. Higher degrees of saturation are noticed above the injection well because liquid is pushed upward and tries to flow back due to gravity. In addition, the limited pore volume of the

overburden is filled with water, leading to pounding and horizontal redistribution of the water. By contrast, all the forces (viscous forces, gravity, and capillary forces) are pointing downward below the injection well, leading to faster fluxes and lower liquid saturations.

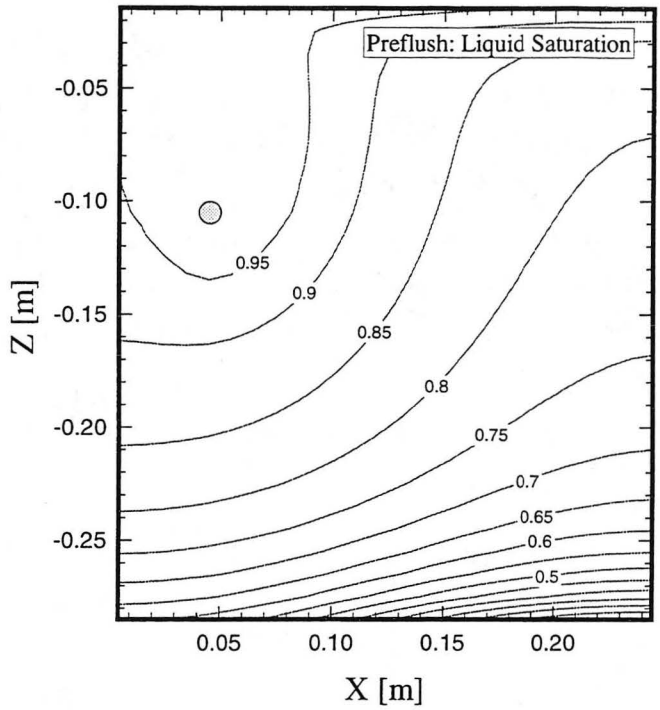

Figure 6: Liquid saturation after preflushing

Performance Measure	Value	Prediction Error
Total mass of preflush liquid [kg]	10.63	5.63
Final injection rate [kg/min]	0.15	0.08
Average liquid saturation around the injection well	0.91	0.02

Table 3: Preflush: Performance measures and prediction errors

The results are summarized in Table 3. A total of 10.63 kg of liquid is injected which corresponds to about 15 pore volumes of the anticipated grout plume. The injection rate at the end of the preflush period is almost constant at 0.15 kg/min. Both the total preflush volume and the injection rate are difficult to predict mainly due to the uncertainty of the absolute

permeability and the fact that the water is injected at a constant pressure rather than at constant rate. In praxis, however, injection time can easily be adjusted until the required volume is pumped into the soil. The average liquid saturation around the injection well is high, assuring almost complete ion exchange.

4.4.3 Primary grout injection

Grout is injected at a constant rate pressure 102 kPa for 8 minutes. The initial viscosity of the grout is 3.7 cp. During injection, the mixture of preflush water and air is displaced by grout. However, the displacement is not piston-like due to capillary pressure gradients and phase dispersion effects which lead to a disperse plume. Furthermore, some mixing between grout and fresh water occurs (by numerical dispersion of X_1^{CS} in the simulation model, by diffusion effects in nature). Figure 7 shows the CS content at the end of the primary grout injection period.

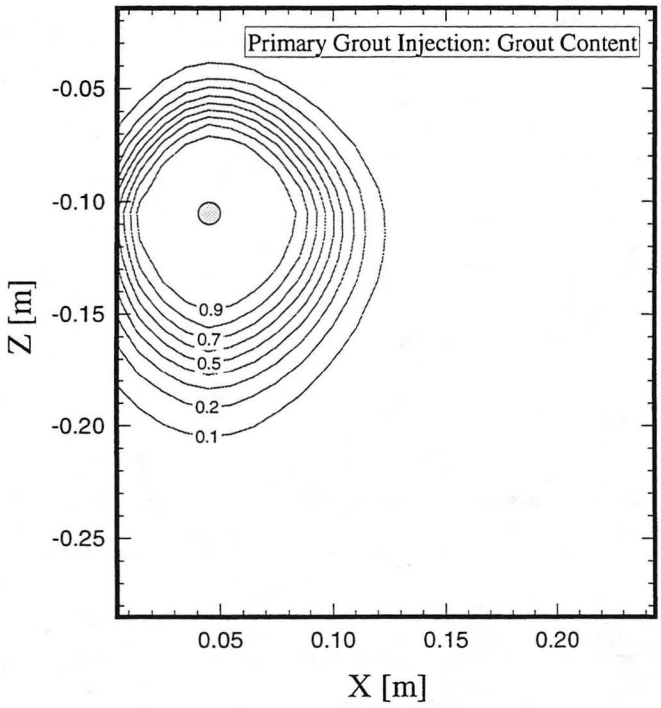

Figure 7: CS content after primary grout injection

Performance Measure	Value	Prediction Error
Total grout mass injected [kg]	0.73	0.39
Center of grout plume, X-coordinate [m]	0.05	0.01
Center of grout plume, Z-coordinate [m]	-0.11	0.02
Spreading of grout plume in X direction [m]	0.03	0.02
Spreading of grout plume in Z direction [m]	0.04	0.03
Average liquid saturation around well	0.90	0.05

Table 4: Primary grout injection: Performance measures and prediction errors

4.4.4 Redistribution

Grout injection stops, and the plume starts slumping under the influence of gravity, and spreading due to capillary forces. The viscosity of the liquid phase increases as a function of time and CS concentration. Pore fluid which does not contain Colloidal Silica drains faster, leading to lower liquid saturations in the areas below and on the side of the grout plume (Figure 8). An almost steady-state grout content distribution is achieved 4 hours after grout injection began (Figure 9). The center of grout mass is located about 4 cm underneath the injection point, and extends about 6 and 10 cm in horizontal and vertical direction, respectively (Table 5). The increase of the plume size is accompanied with a significant reduction of the average liquid saturation from 0.9 to about 0.6. This dispersion effect is mainly driven by capillary forces.

Performance Measure	Value	Prediction Error
Total grout mass injected [kg]	0.73	0.39
Center of grout plume, X-coordinate [m]	0.06	0.02
Center of grout plume, Z-coordinate [m]	-0.16	0.03
Spreading of grout plume in X direction [m]	0.03	0.02
Spreading of grout plume in Z direction [m]	0.05	0.02
Average liquid saturation around well	0.60	0.12

Table 5: Redistribution: Performance measures and prediction errors

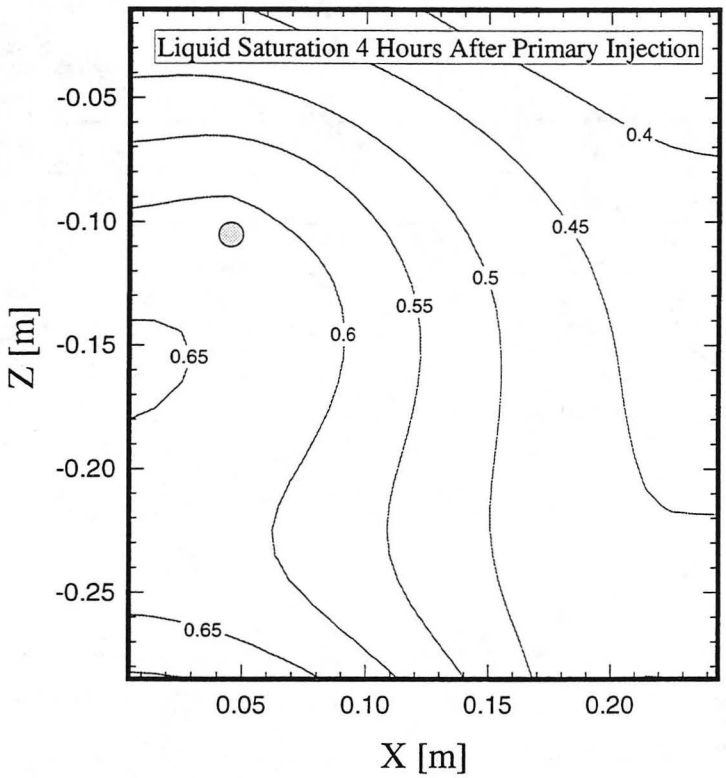

Figure 8: Liquid saturation 4 hours after primary grout injection

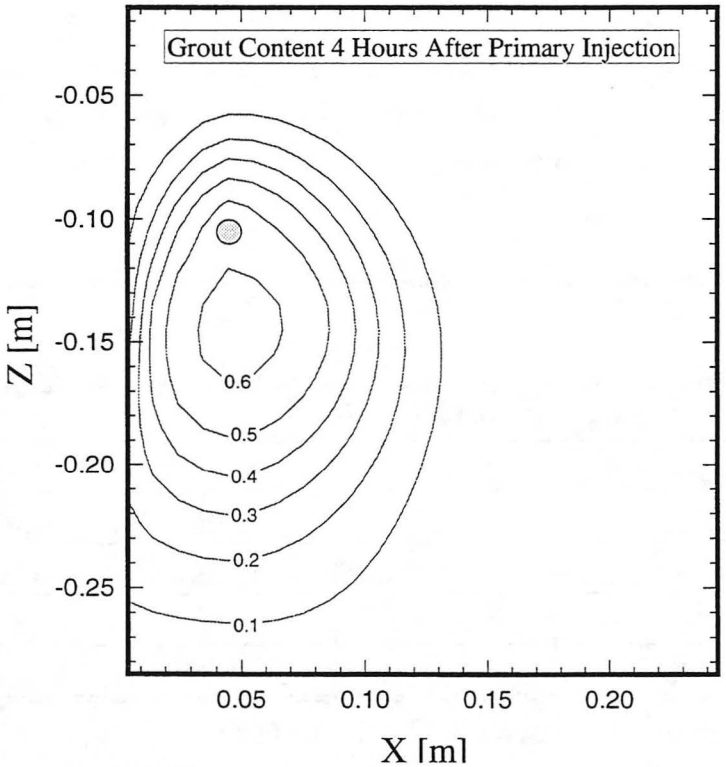

Figure 9: CS content 4 hours after primary grout injection

4.4.5 Solidification

Since the grout plume does not move anymore 4 hours after injection began, we can apply the Solidification Model outlined in Section 3.3. We assume that all the liquid with CS concentrations higher than 0.2 solidifies ($X_{sol} = 0.2$). Column experiments were conducted to investigate permeability reductions from multiple injections of CS grout [*Moridis et al.*, 1994]. These data indicated that permeability reduction is stronger than predicted by gas relative permeability of Brooks-Corey's model (see Equations 5 and 10). Instead, we apply a fourth order model to calculate the permeability of the grouted sand:

$$k_{new} = k_{old} \cdot \left\{ 1 - A \cdot \left[1 - (1 - S_{e,sol})^4 \right] \right\} \tag{16}$$

with

$$S_{e,sol} = \frac{S_{l,sol} - S_{lr}}{1 - S_{lr}} \tag{17}$$

The permeability field is shown in Figure 10. Permeability is reduced by a factor of 65 in the region with the highest grout content, and by a factor of 20 at the fringe of the grout plume. It should be emphasized that these factors highly depend on the solidification model being used, Equation (16). Furthermore, the boundary of the solidified region is defined by the cut-off concentration S_{sol}, which is not well known. The Solidification Model has to be further assessed by measuring permeability reduction factors as a function of grout saturation.

The phase transition during the solidification process leads to a dry-out of the grout plume. As a result, the grouted region exhibits strong capillary forces due to the low liquid saturation and the increase of capillary strength as described by Equation (11). Consequently, water and liquid grout from a secondary injection will be sucked into the remaining pore space if sufficient residual permeability is available. This self-controlling process further reduces the permeability of imperfectly sealed pores.

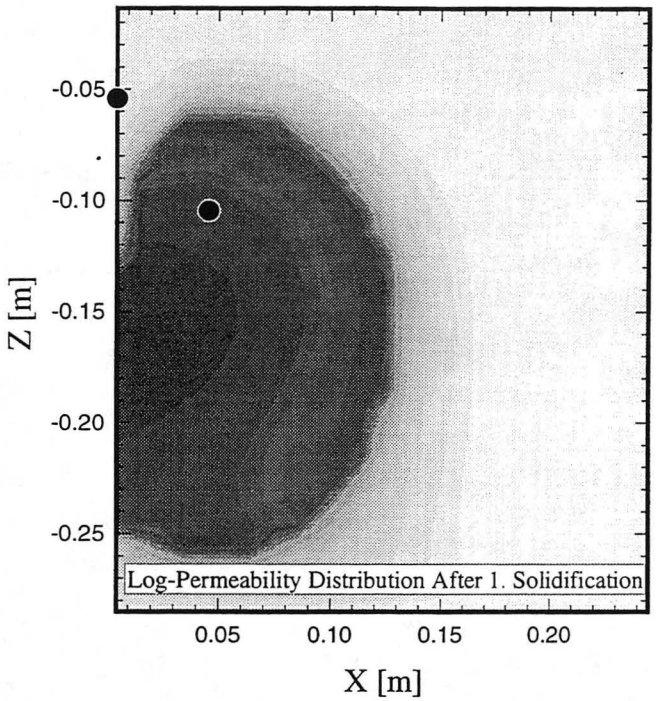

Figure 10: Logarithm of permeability after solidification of primary grout plume

4.4.6 Secondary grout injection

A second grout plume is injected from a borehole centered above the two primary boreholes (see Figure 3). Injection overpressure is 1.5 kPa. A total grout mass of 0.51 kg is injected in 10 minutes. The grout content which originates from the secondary injection is contoured in Figure 11. The grout fills the region between the two primary plumes. Primary and secondary grout plumes merge due to the strong capillary forces. However, deep penetration is inhibited by the low permeability of the grouted soil. This is visualized in Figure 12 which shows the final CS content prior to solidification.

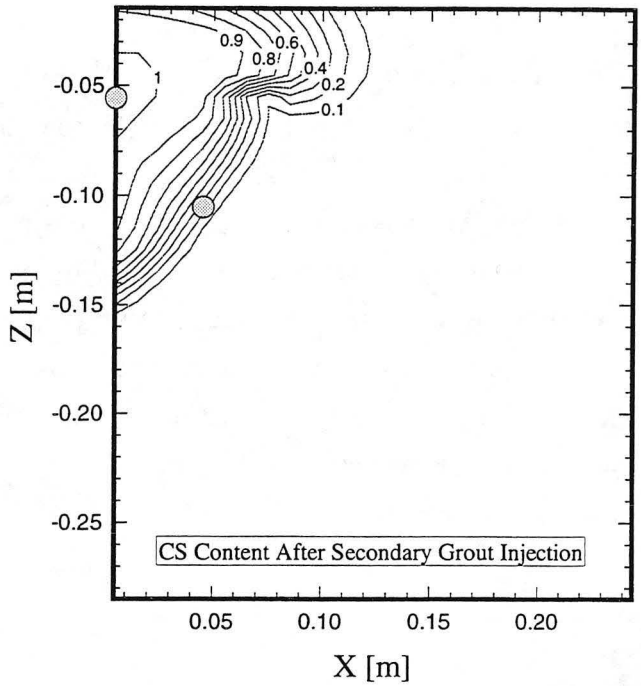

Figure 11: CS content immediately after secondary grout injection

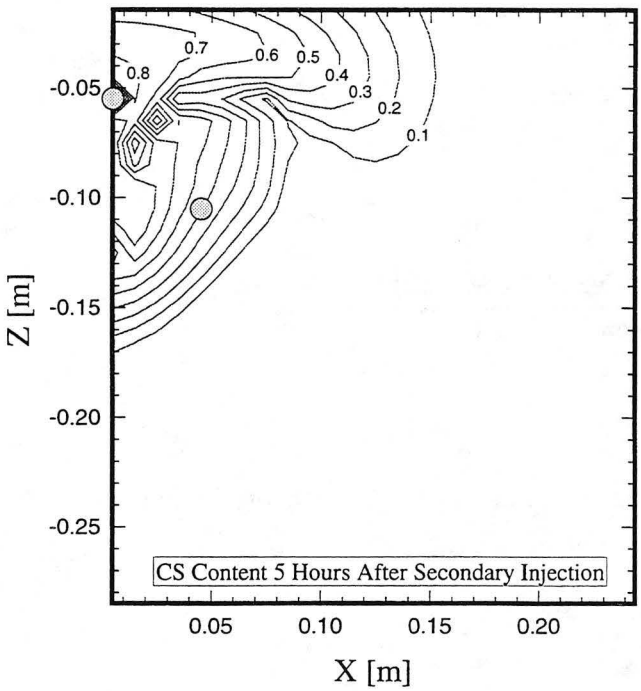

Figure 12: CS content 5 hours after secondary grout injection

4.4.7 Final soil properties

The Solidification Model is applied to determine the characteristics of the repeatedly grouted soil. The final permeability distribution is shown in Figure 13. The region with permeability reductions greater than 3 orders of magnitude is located beneath the secondary well and on the elevation of the primary injection well where the two plumes have penetrated most. These modeling results suggest that a subsurface barrier can be created by multiple injections of CS grout from staggered horizontal wells. After the initial reduction of porosity and permeability, the second injection is more effective because grout is concentrated at the top of the primary plume. In addition, partial penetration of the two plumes assures that weaknesses of the primary plume are cured, leading to a continuous low permeability zone.

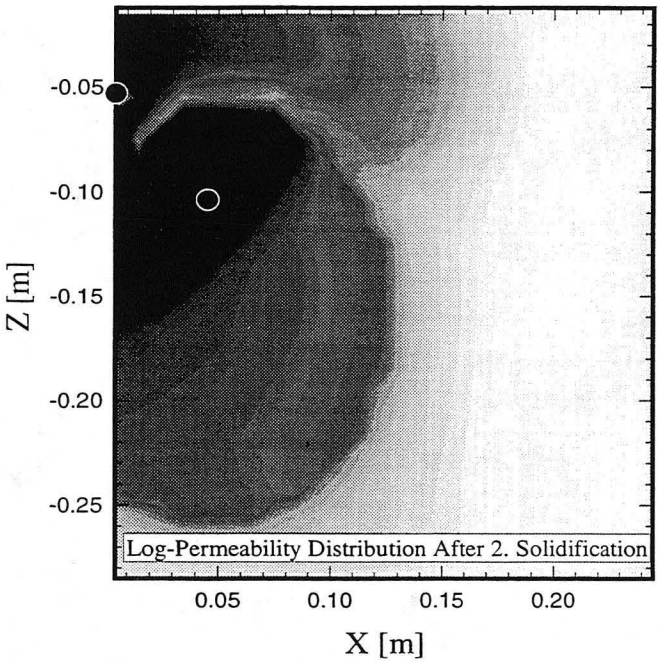

Figure 13: Logarithm of permeability after solidification of secondary grout plume

5. Design Calculations for Field Experiment

5.1 Objectives

Results from scoping calculations (back-of-the-envelope calculations and numerical simulations) are presented for planned field experiment. The objective of the grout injection test is to provide some understanding of how Colloidal Silica (CS) and PolySiloXane (PSX) grouts behave under in-situ conditions. A preliminary assessment of the performance of these fluids as barrier materials will be made based on post injection excavation as well as measurements made during injection.

5.2 Experimental Setup

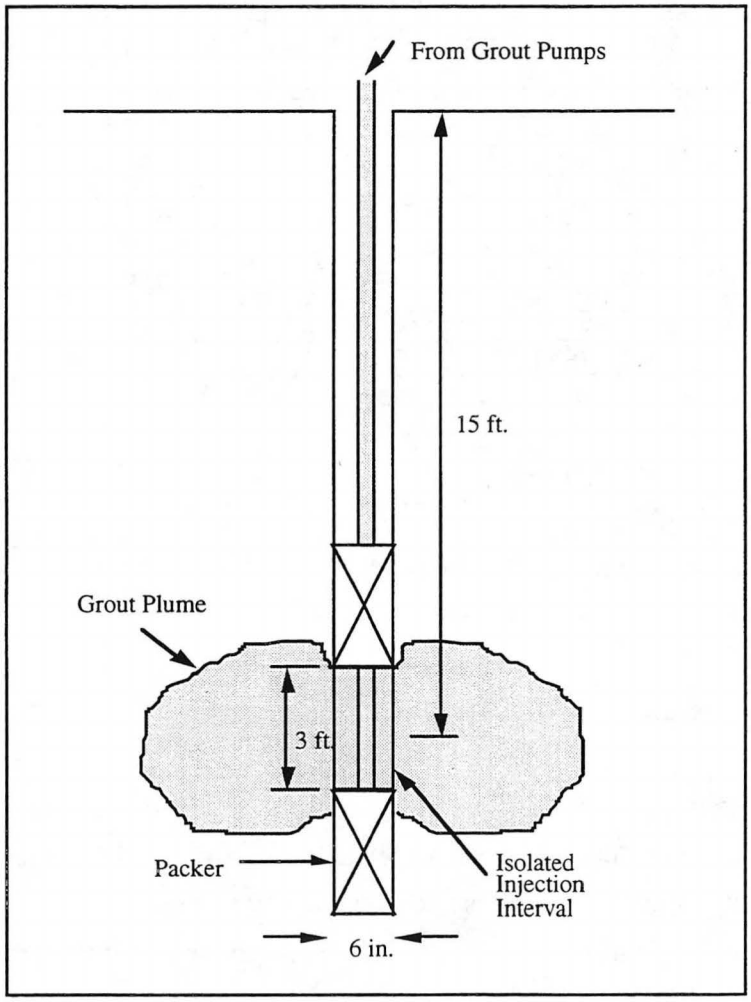

Figure 14: Schematic of borehole setup

The field test involves grout injection from vertical shallow boreholes. A schematic sketch of the borehole test setup is shown in Figure 14. For CS, a preflush will be carried out using a dilute NaCl solution. Grout will be injected under constant pressure conditions for a period of time sufficient to generate a grouted zone about 2 meters in diameter. The corresponding finite difference grid is shown in Figure 15. Note that the flow regime is radial and vertical which yields a two-dimensional radially symmetric mesh.

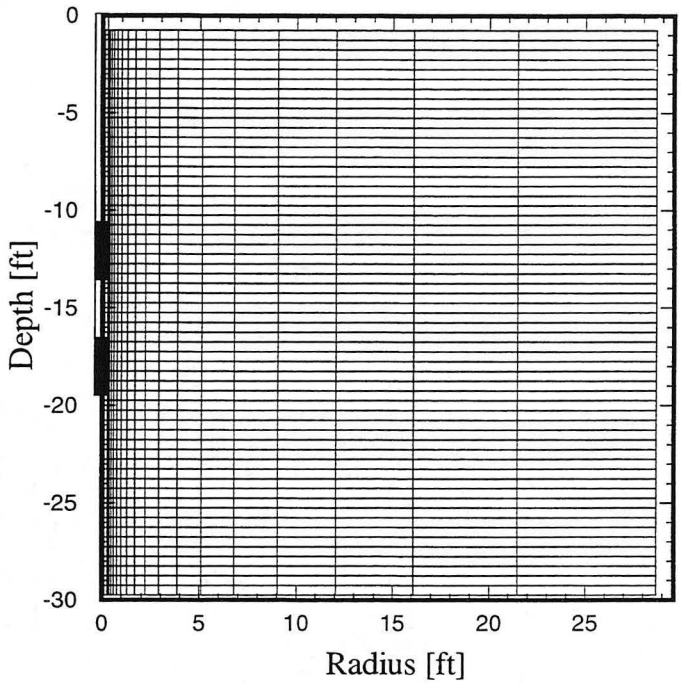

Figure 15: Field experiment: spatial discretization

5.3 Back-of-the-Envelope Calculations

In order to obtain a first guess of the injection times required to emplace a grout plume of a certain extent, a simple analysis is performed assuming single-phase liquid conditions. The results of these calculations will be used to design a test sequence for the numerical model which will take into account effects of capillary forces, gravity, relative permeability, increase of grout viscosity with time, etc.

We consider steady, one-dimensional radial flow from a well in a confined aquifer under single-phase liquid conditions. From Thiem's equation (see e.g. *Bear*, 1979]), the steady-state flow rate is given by

$$Q = k\frac{\rho \cdot g}{\mu} H \frac{2\pi \cdot \Delta s}{\ln(R/r_w)} \tag{17}$$

with

Q	=	flow rate [m^3/s]
k	=	absolute permeability [m^2]
ρ	=	density [kg/m^3]
g	=	gravitational acceleration [m^2/s]
μ	=	viscosity of injected fluid (water or grout) [Pa·s]
H	=	thickness of aquifer [m]
Δs	=	head difference [m]
r_w	=	well radius [m]
R	=	radius of influence [m]

The radius of influence can be approximated by Sichardt's equation:

$$R \approx 3000 \cdot \sqrt{K} \cdot \Delta s \tag{18}$$

where K is hydraulic conductivity [m/s]. The time required to emplace the grout plume can be calculated as follows:

$$t_{inj} = \frac{V}{Q} = \frac{\pi \cdot (r_p^2 - r_w^2) \cdot H \cdot \phi}{Q} \tag{19}$$

with

t_{inj}	=	time required to inject grout [s]
V	=	total grout volume to be injected [m^3]
r_p	=	anticipated radius of grouted soil [m]
ϕ	=	porosity [-]

Equation (19) assumes that the displacement of soil-water by grout is piston-like, and that the pore volume of the grouted zone does not contain residual water, i.e. it is completely saturated with grout.

From Equations (17) - (19) it can be seen that injection time increases

- quadratically with increasing radius of the anticipated grout plume r_p,
- linearly with increasing porosity,
- almost linearly with decreasing injection pressure Δs,
- almost linearly with decreasing permeability,
- linearly with increasing viscosity,
- with decreasing wellbore radius.

Before evaluating Equation (19), we evaluate the range of parameter values to be expected at the potential test site (Table 6).

Parameter	Units	Value	Range
Radius of plume	m	1.00	0.50 - 2.00
Porosity	-	0.40	0.30 - 0.50
Injection pressure	psi	5.00	3.00 - 10.00
Permeability	m^2	10^{-12}	$5 \cdot 10^{-13}$ - $5 \cdot 10^{-12}$
Viscosity preflush	cp	1.00	1.00 - 2.00
Viscosity CS	cp	5.00	2.00 - 10.00
Viscosity PSX	cp	50.00	10.00 - 300.00

Table 6: Parameter ranges for scoping calculations

The plume radius obtained with reasonable injection times will ultimately determine the spacing of wells. If CS grout is used, the soil has to be preflushed with water and a dilute NaCl solution. The amount of preflush water needed to assure sufficient ion exchange is about 10 pore volumes of the anticipated grout plume. The injection pressure is limited by the geostatic pressure of the overburden. The range of permeability is chosen very large because the characteristics of the soil are unknown (see discussion in Section 5.4). Viscosity ranges from 1 cp for preflush fluid over 5 cp for CS to 350 cp PSX [*Persoff*, 1994]. Table 7 summarizes the resulting injection times. The minimum injection time is calculated for the most optimistic parameter combination; the maximum injection time is calculated using the most pessimistic parameter combination. Both values are not realistic, but provide a lower and upper bound.

Test Period	Injection Time [h]	Min. Injection Time	Max. Injection Time
Preflush	72.3	1.6	1968.0
CS Injection	31.6	0.3	832.3
PSX Injection	251.6	1.4	15352.3

Table 7: Injection times required for each test period

It can be seen that injection times (even for the base case parameter set) are unreasonably long for a field application. Provided that the injection time is not allowed to exceed 10 hours, one might backcalculated the conditions under which this requirement can be fulfilled. Some of the parameters are design parameters which can be engineered to a certain extent, whereas others are given by the characteristics of the soil and cannot be changed. The two parameter subject to engineering design are the plume size and the initial viscosity of the grout. Soil parameters are permeability and porosity. While the injection pressure can be prescribed by the engineer, its upper limit is given by the soil properties and the depth of the injection. The following sensitivity study examines the injection time for CS emplacement. Three of the five parameters under consideration are fixed, and two are varied in order to see for which parameter combination the anticipated injection time of 10 hours can be achieved. The new parameter set is summarized in Table 8.

Parameter	Value	Comment
Radius of plume [m]	variable	as large as possible
Porosity [-]	0.40	relatively certain, linear impact
Injection pressure [psi]	10.00	increased to upper limit
Permeability [m^2]	variable	highly uncertain
Viscosity of CS [Pa·s]	2.00	reduced by diluting grout [*Persoff*, 1994]

Table 8: Reasonable parameter set leading to reduced injection times

The resulting injection times for a CS grout is shown in Figure 16. Injection time is contoured as a function of permeability and anticipated grout plume radius. The diagram can be used to inversely determine the size of the plume for a given permeability and injection

time. For example, if the permeability is one darcy, the radius of the plume is 0.5 m after 2 hours of constant head injection at 10 psi. It has a radius of 1.15 m after an injection time of 10 hours. If the permeability is below $0.5 \cdot 10^{-12}$ m^2, the grouted plume is smaller than 0.8 m radius for a 10 hour injection time. In order to examine different cases, the times shown in Figure 16 have to be multiplied by one or a combination of the factors listed in Table 9.

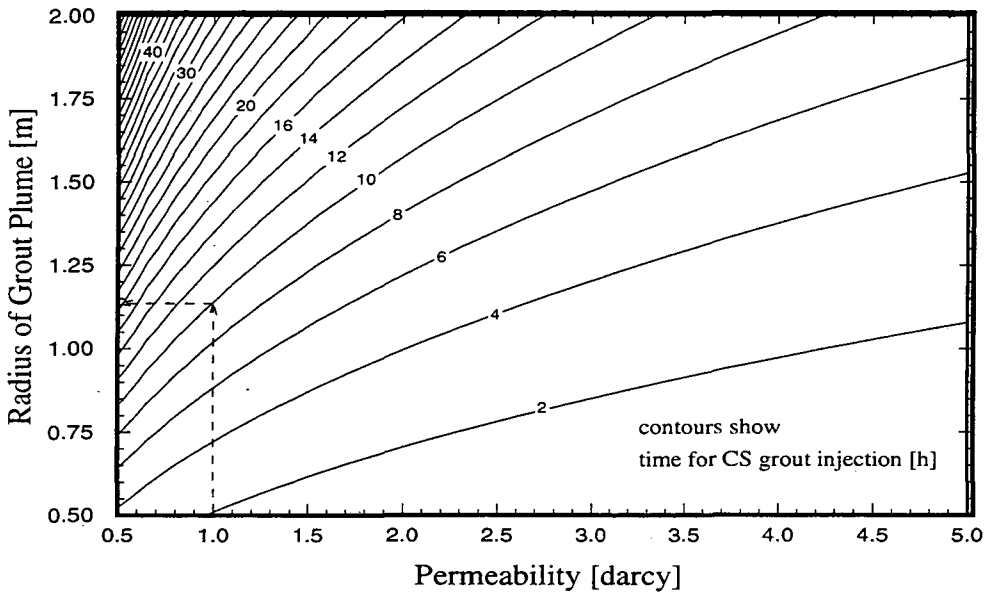

Figure 16: CS grout injection time as a function of permeability and plume size

Multiply times by Factor in order to obtain time needed ...	Factor
for preflush with 10 PV of dilute NaCl solution	5.0
for CS injection	1.0
for PSX injection	25.0
if an injection pressure of X [psi] is used	10.0/X
if grout of a viscosity of X [cp] is used	X/2.0
if porosity is X	X/0.4

Table 9: Correction factors to calculate injection times

Recall that these estimates are based on various assumptions which are different from those encountered in an unsaturated medium during transient flow under gravity and capillary forces. In order to assess the simple scoping calculations presented in this Section, CS grout injection is numerically modeled as discussed below.

5.4 Soil Characteristics

Hydrogeologic parameters of the soil at the potential test site are not available. However, particle size distributions for a sand and a gravel gradation were measured. In addition, the hydraulic properties of the sediments at the Hanford site were extensively studied in the past. By comparing the sieve analysis with the particle size distributions published in *Connelly et al.* [1992a,b] and *Rockhold et al.* [1993], we determined the value and range of each hydraulic parameter needed for the modeling study. However, since no precise sieve analysis is available for the fine particles in the soil which determine the soil's permeability, the numbers obtained from this comparison are highly uncertain. The parameter set is summarized in Table 10. Van Genuchten's characteristic curves are chosen to describe relative permeability for liquid and gas, k_{rl} and k_{rg}, and capillary pressure p_c as a function of liquid saturation S_l [*Luckner et al.*, 1989]:

$$p_c = \frac{1}{\alpha} \cdot \left(S_e^{-1/m} - 1\right)^{1-m} \tag{20}$$

$$k_{rl} = S_e^{1/2} \cdot \left[1 - (1 - S_e^{1/m})^m\right]^2 \tag{21}$$

$$k_{rg} = (1 - S_e)^{1/3} \cdot \left[1 - S_e^{1/m}\right]^{2m} \tag{22}$$

with

$$S_e = \frac{S_l - S_{lr}}{1 - S_{lr}} \tag{23}$$

$$m = 1 - 1/n \tag{24}$$

In this form, van Genuchten's curves contain three adjustable parameters: $1/\alpha$ (air entry pressure), n (pore size distribution index), and S_{lr} (residual liquid saturation).

Parameter	Value
log (absolute permeability [m^2])	-12.00
vG parameter n [-]	1.50
log (vG parameter $1/\alpha$ [bar])	-1.30
initial gas saturation S_{g0} [-]	0.60
initial viscosity of grout μ_0 [cp]	2.00
gel time [h]	24.00
porosity ϕ [-]	0.40
residual liquid saturation S_{lr} [-]	0.30

Table 10: Parameter set for field experiment

5.5 Results

The system behavior of each test period can be described as follows:

(1) *Initial and boundary conditions*:
The soil is initially dry with a uniform liquid saturation of 40 % with a capillary suction of 0.24 MPa. Humid air is allowed to enter the soil from the surface and from the borehole above the upper packer. No flow boundary conditions are applied around the packers, at the right and at the bottom of the model domain. Initial gas pressure is 0.1 MPa.

(2) *Preflushing period*
Water is injected at a constant overpressure of 10 psi for 30 hours. Contours of liquid saturation and excess pressure at the end of the preflush period are shown in Figure 17.

(3) *Grout injection period*
Grout is injected at a constant overpressure of 10 psi for 10 hours. The initial viscosity of the grout is 2 cp. During injection, the mixture of preflush-water and air is displaced by grout. However, the displacement is not piston-like due to capillary pressure gradients and phase dispersion effects which lead to a disperse plume. Furthermore,

some mixing between grout and fresh water occurs. Figure 18 shows liquid saturation and CS content at the end of the grout injection period. Recall that the radius of the grout plume has been predicted to be approximately 1.15 m ≈ 3.8 ft by means of simple scoping calculations (see Figure 16). This is in surprisingly good agreement with the results from the numerical model. The pressure distribution is shown in Figure 19. Note that the region of increased pore pressures is smaller compared to the one at the end of the preflush period due to the higher viscosity of the injected fluid. Flow rates during preflushing and grout injection are shown in Figure 20. The drop of injection rate when switching from preflushing to grout injection is due to the increased viscosity of the gel. The grout injection rate is almost constant leading to a linear increase of the total grout mass in the soil.

(4) *Redistribution and gelling period*

Grout injection stops, and the plume starts slumping due to gravity, and spreading due to capillary forces. Simulation stops 66 hours after grout injection began. The final distribution of liquid saturation and gel content is shown in Figure 21. The plume has slumped down by about 1.8 ft. Overpressures are completely dissipated. The results are summarized in Table 11.

Performance measure	Value
Total grout mass injected [kg]	2773.80
Center of grout mass, Z coordinate [ft]	-16.82
Spread of grout plume in Z direction [ft]	1.72
Average grout content [-] in region 0.3 < R < 6.0 ft, -16.5 < Z < -13.5 ft	0.64
Flow rate at the end of preflushing [kg/s]	0.12
Flow rate at the end of grout injection [kg/s]	0.07

Table 11: Model results field experiment

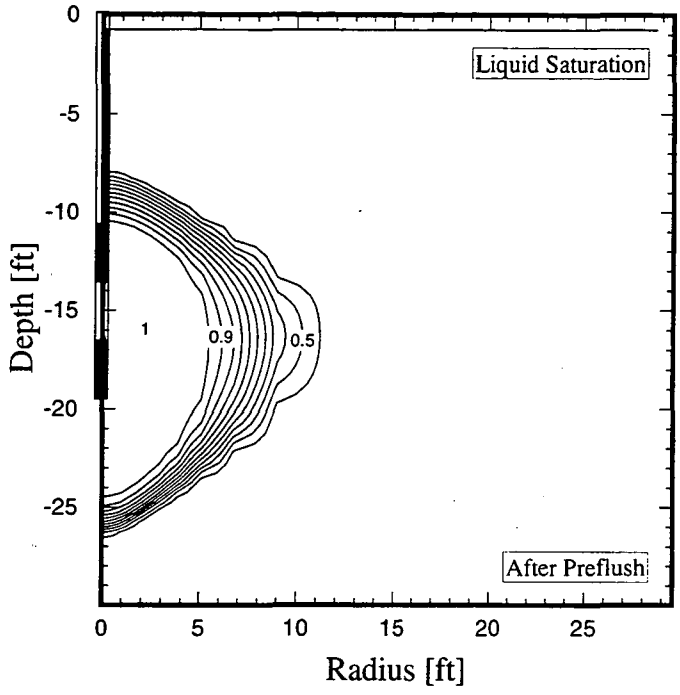

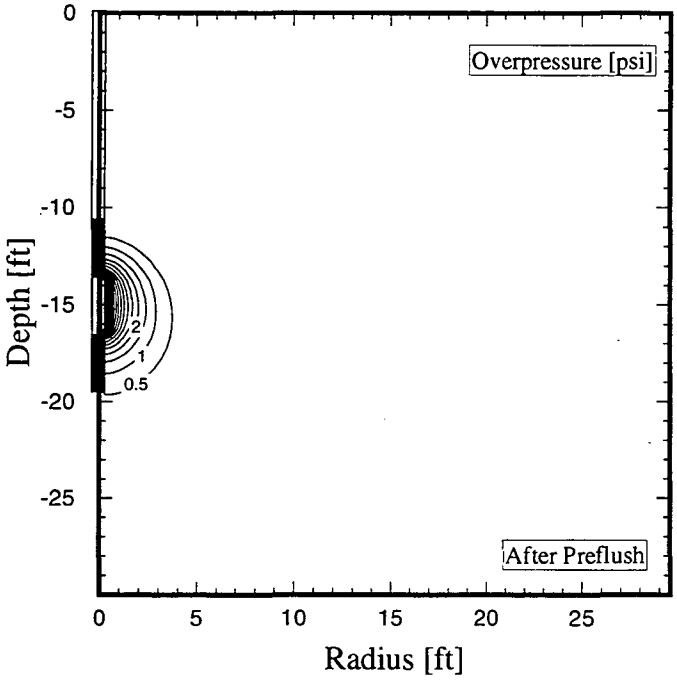

Figure 17: Liquid saturation and pressure distribution after preflushing

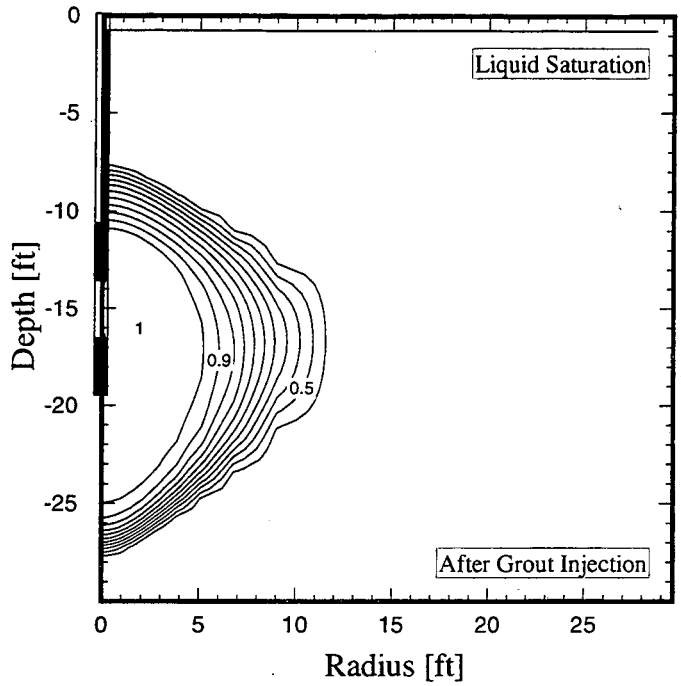

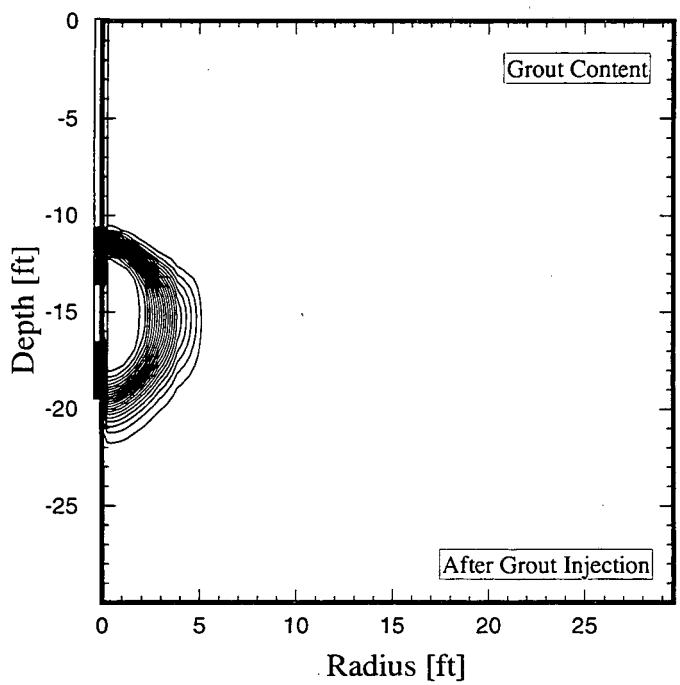

Figure 18: Liquid saturation and CS content at the end of the grout injection period

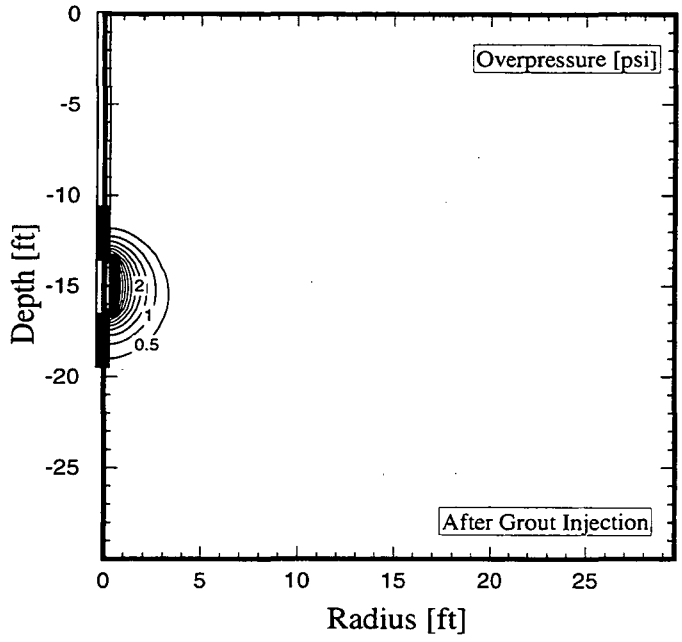

Figure 19: Pressure distribution at the end of the grout injection period

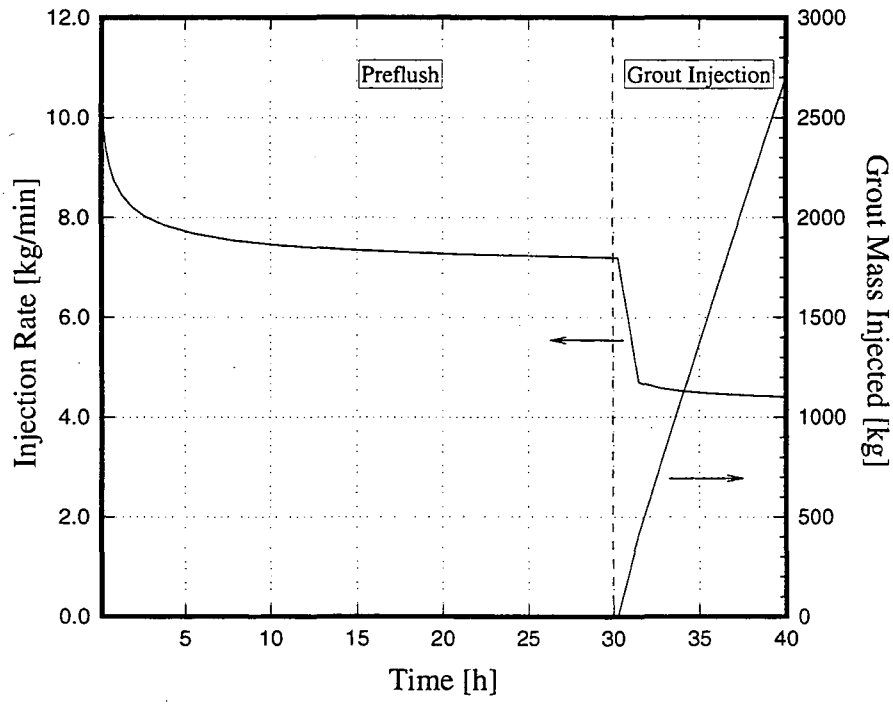

Figure 20: Flow rates and total grout mass injected

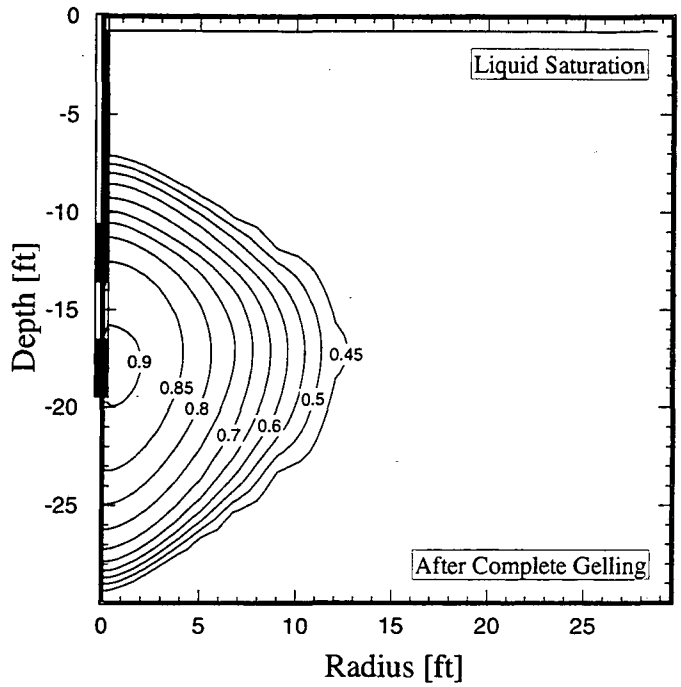

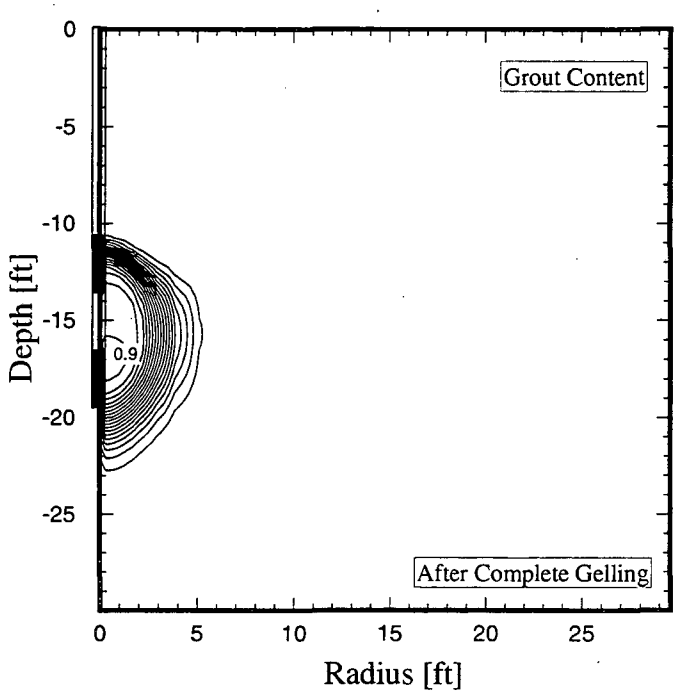

Figure 21: Liquid saturation and grout content at the end of the gelling period

The Solidification Model (see Section 3.4) is applied to obtain a first estimate of the permeability reduction obtained by the injection of the chemical grout. The permeability is reduced by at least an order of magnitude in a spherical region about 5 ft in diameter. Larger reductions can be obtained by multiple injections, leading to higher grout contents and lower porosities once the grout has completely gelled.

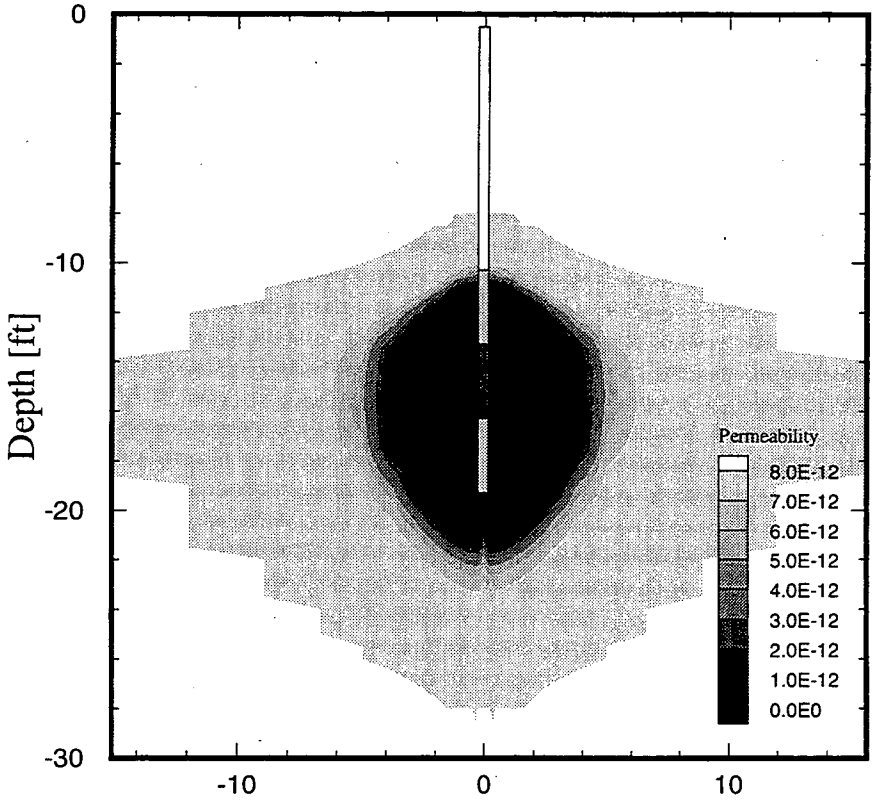

Figure 22: Permeability distribution after grout solidified

6. SUMMARY AND CONCLUDING REMARKS

The emplacement of liquids under controlled viscosity conditions is investigated by means of numerical simulations. Design calculations were performed for a laboratory experiment on a decimeter scale, and a field experiment on a meter scale. The purpose of the laboratory experiment was to study the behavior of multiple grout plumes when injected in a porous medium. The calculations for the field trial aim at designing a grout injection test from a vertical well in order to create a grout plume of a significant extent in the subsurface.

In our modeling approach, the grout is treated as a miscible fluid the viscosity of which is a function of time and concentration of the gelling agent in the pore water. If a certain high viscosity is reached and the movement of the grout plume ceases, the gel is assumed to solidify instantaneously, leading to a new porous medium with reduced porosity and permeability.

The characteristic curves of the ungrouted sand are derived from a water retention curve measured in the laboratory, and from values found in the literature for similar soils. The gel-time curve (viscosity of pure grout as a function of time) used in the simulations is based on laboratory measurements. A simple mixing-rule is applied to account for dilution of the injected grout with pore water. A Solidification Model has been developed which provides the properties of the soil after the grout has been cured.

Modeling the laboratory experiment (see Section 4) has generated some insight into the flow of fluids with increasing viscosity under the influence of gravity and capillary forces. The saturation within the immobilized grout plume may be significantly below one, leading to an incomplete ceiling of the pore space. However, when multiple injections are performed, relatively high conductive pathways are preferentially filled with grout, assuring a sufficient permeability reduction after the grout has cured. The calculated properties of the subsurface barrier strongly depend on the validity of the Solidification Model proposed in this study. Additional research is needed to assess the relationship between final grout content and permeability reduction. Conceptual models have to be developed which predict capillary pressure and relative permeability of the grouted soil.

Modeling the planned field test (see Section 5) has revealed that emplacement of a grout plume of a certain extent may require long injection times if the permeability of the soil is low. A low initial grout viscosity is essential to facilitate reasonable injection times. These

conclusions are based on the assumption that the permeability of the soil at the potential test site is in the order of 10^{-12} m^2. Soils beneath the Hanford tanks exhibit these properties. The comparison between numerical simulations and back-of-the-envelope calculations have shown that simple formulas are sufficiently accurate to obtain a first estimate of injection times and plume sizes. This is especially true for low permeable soils where gravitational slumping and spreading of the plume due to capillary forces are not significant processes within the time frame of interest.

ACKNOWLEDGMENT

This work is supported the U.S. Department of Energy, Office of Environmental Management, Office of Technology Development, under contract DE-AC03-76SF00098. We would like to thank C.M. Oldenburg and A. Datta-Gupta for their careful reviews of the manuscript.

REFERENCES

Bear, J., Hydraulics of groundwater, McGraw-Hill Inc., New York, 1979.

Brooks, R. H., and A. T. Corey, Hydraulic properties of porous media, Hydrology Papers, Colorado State University, Fort Collins, Colorado, 1964.

Burdine, N. T., Relative permeability calculations from pore-size distribution data, *Trans. Am. Inst. Min. Metall. Pet. Eng.*, 198, 71-78, 1953.

Connelly, M. P., B. H. Ford, and J. V. Borgese, Hydrogeologic model for the 200 west groundwater aggregate area, WHC-SD-EN-TI-014, Westinghouse Hanford Company, Richland, Washington, 1992a.

Connelly, M. P., B. H. Ford, J. V. Borgese, S. Trent, and J. Lindberg, Hydrogeologic model for the 200 east groundwater aggregate area, WHC-SD-EN-TI-019, Westinghouse Hanford Company, Richland, Washington, 1992b.

Finsterle, S., ITOUGH2 User's Guide, Lawrence Berkeley Laboratory Report LBL-34581, Berkeley, CA , 1993.

Iler, R. K., The chemistry of silica, Wiley-Interscience, New York, 1979.

International Formulation Committee, A formulation of the thermodynamic properties of ordinary water substance, IFC Secretariat, Düsseldorf, Germany, 1967.

Luckner, L., M. Th. van Genuchten, and D. Nielsen, A consistent set of parametric models for the two-phase flow of immiscible fluids in the subsurface, *Water Resour. Res.*, 25 (10), 2187-2193, 1989.

Moridis, G. J., P. Persoff, H.-Y. Holman, S. J. Muller, K. Pruess, P. Witherspoon, and C. J. Radke, Containment of contaminants through physical barriers formed from viscous liquids emplaced under controlled viscosity conditions, FY 1993 Annual Report, Lawrence Berkeley Laboratory Report LBL-29400, Berkeley, CA, 1994.

Persoff, P., Preliminary grout formulas for field testing, Memorandum, January 6, 1994.

Pruess, K, TOUGH2 - A general-purpose numerical simulator for multiphase fluid and heat flow, Lawrence Berkeley Laboratory Report LBL-29400, Berkeley, CA, 1991a.

Pruess, K., EOS7, An equation-of-state module for the TOUGH2 simulator for two-Phase flow of saline water and air, Lawrence Berkeley Laboratory Report LBL-31114, Berkeley, CA, 1991b.

Pruess, K., Grid orientation and capillary pressure effects in the simulation of water injection into depleted vapor zones, *Geothermics*, 20(5/6), 257-277, 1991c.

Pruess, K., Dispersion of immiscible fluid phases in gravity-driven flow: A Fickian diffusion model, submitted to Water Resources Research, Lawrence Berkeley Laboratory Report LBL-33914, Berkeley, CA, 1993.

Rockhold, M. L., M. J. Fayer, and P. R. Heller, Physical and hydraulic properties of sediments and engineered materials associated with grouted double-shell tank waste disposal at Hanford, PNL-XXXX, UC-510 Draft Report, 1993.

van Genuchten, M. Th., A closed-form equation for predicting the hydraulic conductivity of unsaturated soils, *Soil Sci. Soc. Am. J.*,44, 892-898, 1980.

Ernest Orlando Lawrence Berkeley National Laboratory
One Cyclotron Road | Berkeley, California 94720

Prepared for the U.S. Department of Energy under Contract No. DE-AC03-76SF00098

AAX271
LBL Libraries